DROPS: DEEP RETRIEVAL OF PHYSIOLOGICAL SIGNALS VIA ATTRIBUTE-SPECIFIC CLINICAL PROTOTYPES

Anonymous authors
Paper under double-blind review

ABSTRACT

The ongoing digitization of health records within the healthcare industry results in large-scale datasets. Manually extracting clinically-useful insight from such datasets is non-trivial. However, doing so at scale while simultaneously leveraging patient-specific attributes such as sex and age can assist with clinical-trial enrollment, medical school educational endeavours, and the evaluation of the fairness of neural networks. To facilitate the reliable extraction of clinical information, we propose to learn embeddings, known as clinical prototypes (CPs), via supervised contrastive learning. We show that CPs can be efficiently used for large-scale retrieval and clustering of physiological signals. We also show that CPs capture attribute-specific semantic relationships.

1 INTRODUCTION

Physiological data are being collected at a burgeoning rate. Such growth is driven by the digitization of previous patient records, the presence of novel monitoring systems, and the recent recommendation to facilitate the exchange of health records (European Commission, 2019). This engenders large-scale datasets from which the manual extraction of clinically-useful insight is non-trivial.

In the presence of large-scale datasets, retrieving instances based on some user-defined criteria has been a longstanding goal within the machine learning community. This information retrieval (IR) process typically consists of a query that is used to search through a large database and retrieve matched instances. Within healthcare, the importance of an IR system is threefold. First, it provides researchers with greater control over which patients to choose for clinical trial recruitment. Second, IR systems can serve as an educational and diagnostic tool, allowing physicians to identify seemingly similar patients who exhibit different clinical parameters and vice versa. Lastly, if the query were to consist of sensitive attributes such as sex, age, and race, then such a system would allow researchers to more reliably evaluate the individual and counterfactual fairness of a particular model (Verma & Rubin, 2018). To illustrate this point, let us assume the presence of a query instance that corresponds to a patient with an abnormality of the heart, atrial fibrillation, who is male and under the age of 25. To reliably determine the sensitivity of a model with respect to sex, one would observe its response when exposed to a counterfactual instance, namely the exact same instance *but* with a different sex label (Kusner et al., 2017). At present, IR systems within the healthcare domain fail to incorporate such patient-specific attributes.

Several researchers have implemented IR systems to retrieve instances from the electronic health records (Wang et al., 2019; Chamberlin et al., 2019). However, most of these approaches do not incorporate an attribute-specific search and do not trivially extend to physiological signals. Instead, we propose to learn embeddings, referred to as clinical prototypes (CPs). CPs are efficient descriptors of a combination of patient-specific attributes, such as disease, sex, and age. We learn these embeddings via contrastive learning whereby representations of instances are encouraged to be similar to their corresponding clinical prototype and dissimilar to the others. To the best of our knowledge, we are the first to design a contrastive learning based large-scale retrieval system for physiological signals.

Contributions. Our contributions are the following:

- **Attribute-specific clinical prototypes** - we propose a supervised contrastive learning framework to learn embeddings, referred to as clinical prototypes (CPs), that are efficient descriptors of a set of patient attributes, e.g., disease, sex, and age.
- **Deep retrieval and clustering** - we exploit CPs to retrieve instances corresponding to a specific patient-attribute combination and assign instances to various clusters.

2 Related Work

Clinical representation learning involves representing clinical data in a way that is meaningful for solving tasks. Most research attempts to learn representations of electronic health records (EHRs) (Miotto et al., 2016; Huang et al., 2019; Liu et al., 2019; Li et al., 2020b; Biswal et al., 2020; Darabi et al., 2020; Landi et al., 2020) and medical text (Si & Roberts, 2019) in a generative manner. For example, both Landi et al. (2020) and Huang et al. (2019) implement an autoencoder to learn patient representations. These representations are then clustered either in a hierarchical manner or via K-means. Other methods involve learning prototypes. For example, Li et al. (2020a) propose to do so via the ProtoNCE loss. Our approach, unlike theirs, exploits readily-available patient-attribute data and is not dependent upon the K-means algorithm. Moreover, Van Looveren & Klaise (2019) learn to perturb prototypes to derive interpretable counterfactual instances. Most similar to our work is that of Garnot & Landrieu (2020) where the distance between class prototypes, which are learned in an end-to-end manner, is regularized based on a pre-defined tree hierarchy. In contrast, we learn attribute-specific prototypes via supervised contrastive learning and capture their semantic relationships via distance-based regularization.

Clinical information retrieval whereby instances similar to a query are retrieved was first introduced in 1990 (Hersh & Greenes, 1990). Most research in this domain revolves around text (Gurulingappa et al., 2016; Wang et al., 2017; Rhine, 2017; Wallace et al., 2016). For example, D'Avolio et al. (2010) map text to SNOMED concepts to retrieve clinical documents. More recently, IR has been performed with biomedical images, and is referred to as content-based image retrieval (Saritha et al., 2019; Chittajallu et al., 2019). Others have extended this concept to EHR data (Goodwin & Harabagiu, 2018; Wang et al., 2019; Chamberlin et al., 2019). For example, Chamberlin et al. (2019) implement rudimentary IR methods such as divergence from randomness on the UPMC and MIMIC III (Johnson et al., 2016) datasets with the aim of discovering patient cohorts. In contrast to such methods, we implement a deep-learning based clinical information retrieval system for physiological signals.

3 Methods

3.1 Attribute-specific Clinical Prototypes

We aim to design a framework that can be exploited for *both* the retrieval and clustering of physiological signals. In the process, we exploit readily-available patient attribute information, such as disease, sex, and age. This is driven by our desire to imbue the retrieval and clustering processes with attribute-specific information. To that end, we propose to learn a set of embeddings, $p \in P$, where $|P| = M$, representing each of the M possible patient-attribute combinations within a dataset. More specifically, each embedding, p, describes a set of attributes, $A = \{\alpha_1, \alpha_2, \alpha_3\}$ where $\alpha_1 = \text{disease}$, $\alpha_2 = \text{sex}$ and $\alpha_3 = \text{age}$. As a result, we refer to these embeddings as attribute-specific clinical prototypes or CPs. We propose to learn such CPs via contrastive learning, a primer of which is provided next.

3.2 Contrastive Learning

Assume the presence of a learner, $f_\theta : x \in \mathbb{R}^D \rightarrow v \in \mathbb{R}^E$ parameterized by θ, that maps a D-dimensional input, x, to an E-dimensional representation, v. A pair of representations, $v_1 = f_\theta(x_1)$ and $v_2 = f_\theta(x_2)$, are said to constitute a positive pair if they share some context. Such shared context can refer to representations that belong to the same disease, sex, or age group. In contrastive learning, representations within a positive pair are attracted to one another and repelled from all other representations. In doing so, representations learn to become invariant to subtle differences in each of the aforementioned groups. Such invariance can be beneficial when learning an efficient descriptor of a particular group.

3.3 LEARNING ATTRIBUTE-SPECIFIC CLINICAL PROTOTYPES

We aim to learn clinical prototypes that efficiently describe a set of attributes. To do so, we attract each representation of an instance associated with a set of attributes to the CP that describes that same set. This can be achieved in two ways.

Hard assignment. We encourage each representation, v_i, of an instance, x_i, associated with a particular set of attributes, A, to be similar to the single clinical prototype, p_A, that describes the exact same set of attributes, and dissimilar to the remaining clinical prototypes p_j, where $j \neq A$. We quantify this similarity, $s(v_i, p_A)$, using the cosine similarity, with a temperature parameter, τ_s. Mapping each representation to a *single* CP is referred to as a hard assignment. To encourage this behaviour, one would optimize the following objective function for a mini-batch of size, B:

$$\mathcal{L}_{contrastive-hard} = -\frac{1}{B}\sum_{i=1}^{B}\log\left(\frac{e^{s(v_i,p_A)}}{\sum_j^M e^{s(v_i,p_j)}}\right) \tag{1}$$

$$s(v_i, p_A) = \frac{v_i \cdot p_A}{\|v_i\|\|p_A\|} \cdot \frac{1}{\tau_s} \tag{2}$$

Soft assignment. For each representation, v, the hard assignment approach assumes a bijective relationship with p. This suggests that CPs without a perfect attribute match (i.e., a near miss) do not leverage potentially useful information from these representations. As such, we propose a soft assignment approach whereby each representation, v_i, is attracted to a *subset* of class-specific clinical prototypes, L, where $L \subset P$. We opted for this class-specific setup to avoid erroneously attracting representations to CPs from a different class.

Recall, though, that the CPs in L still describe different sets of non-class attributes, and thus should not be attracted to each representation to the same extent. Doing so would collapse the CPs to a single point, eradicating the principal desideratum of attribute-specific descriptors (see Appendix A). To avoid such collapse, we modulate the attraction between each representation, v_i, and each clinical prototype, p_k, by introducing a weight, w_{ik}. We chose this weight to be dependent on the discrepancy between the attribute sets, $d(A_i, A_k)$. In other words, there is greater attraction for more similar attribute sets (see Fig. 1). Mathematically, we extend Eq. 1 as follows:

$$\mathcal{L}_{contrastive-soft} = -\frac{1}{B}\sum_{i=1}^{B}\left[\sum_{k=1}^{M}\omega_{ik}\log\left(\frac{e^{s(v_i,p_k)}}{\sum_j^M e^{s(v_i,p_j)}}\right)\right] \tag{3}$$

$$\omega_{ik} = \begin{cases} \frac{e^{d(A_i,A_k)}}{\sum_j^{|L|} e^{d(A_i,A_j)}} & \text{if class}_i = \text{class}_k \\ 0 & \text{otherwise} \end{cases} \tag{4}$$

$$d(A_i, A_k) = [\delta(\text{class}_i = \text{class}_k) + \delta(\text{sex}_i = \text{sex}_k) + \delta(\text{age}_i = \text{age}_k)] \cdot \frac{1}{\tau_\omega} \tag{5}$$

where δ is the Kronecker delta function that evaluates to one if the argument is true and zero otherwise and τ_ω is a temperature parameter that determines how soft the assignment is. For example, as $\tau_\omega \to 0$, the loss-term approaches the hard assignment formulation.

Arrangement of clinical prototypes. Clinical prototypes learned in an end-to-end manner as presented will exhibit a high and desirable degree of *inter-cluster* separability. However, prototypes *within* a cluster are still at risk of collapsing to a single point. This would decrease their utility for attribute-based querying of instances. Therefore, to encourage CPs to exhibit *intra-cluster* separability and adopt the formation shown in Fig. 1, we propose a distance-based regularization term, calculated as follows. First, we normalize all CPs in the set, P, using the L_2 norm and calculate their pairwise Euclidean distance, generating the matrix $\hat{D} \in \mathbb{R}^{M\times M}$ (Fig. 1 right). As we are only interested in the pairwise distances for prototypes *within* the same cluster, we generate sub-matrices, $D_c \in \mathbb{R}^{M/C\times M/C}$ with $c \in [1, \ldots, C]$ where C is the number of class-specific clusters, each populated with ground-truth distances, d_E. We design such distances to reflect the semantic relationship between the attribute sets of CPs. More specifically, $d_E = \beta \times S$ where $\beta \in \mathbb{R}$ is a user-defined distance and $S \in \mathbb{Z}^+$ is the integer distance between attributes. For example, a pair of

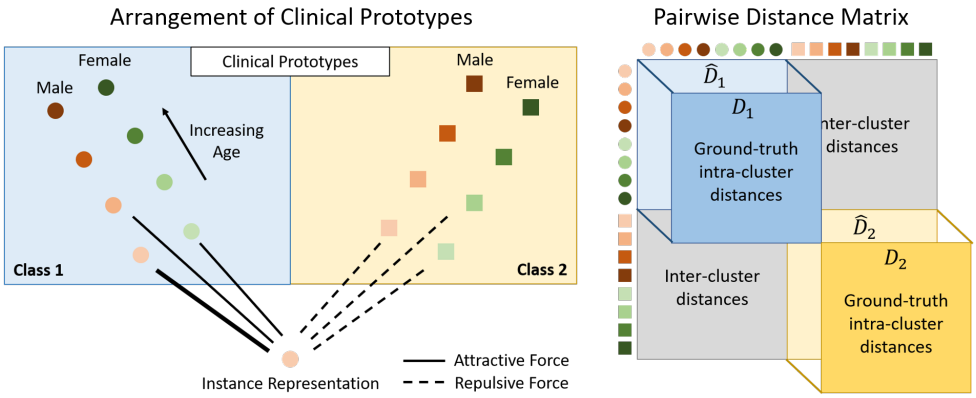

Figure 1: **Left.** Visualization of the attractive and repulsive forces present between an instance representation and clinical prototypes that belong to two different clusters/classes. The clinical prototypes are coloured according to sex and shaded in ascending order of age. All repulsive forces are treated equally whereas attractive forces are weighted according to the degree of attribute matching between the instance and the respective clinical prototype. **Right.** Matrix $\hat{D} \in \mathbb{R}^{|M| \times |M|}$ illustrating the Euclidean distance between each pair of clinical prototypes. The mean-squared error between the observed intra-cluster distances, $\hat{D}_c$, and the ground-truth intra-cluster distances, D_c, is minimized.

CPs that differ according to sex with $A_1 = \{\text{AFIB}, \text{M}, < 25\}$ and $A_2 = \{\text{AFIB}, \text{F}, < 25\}$, result in $S = 1$ and $d_E = \beta \times 1$. We then calculate the mean-squared error between, $\hat{D}_c$, corresponding to the actual distances between class-specific CPs, and D_c, corresponding to the ground-truth distances. Our final objective function thus includes the soft contrastive loss (Eq. 3) and the regression loss.

$$\mathcal{L}_{regression} = \frac{C}{M^2} \sum_{c=1}^{C} (\hat{D}_c - D_c)^2 \tag{6}$$

$$\mathcal{L}_{combined} = \mathcal{L}_{contrastive-soft} + \mathcal{L}_{regression} \tag{7}$$

4 Experimental Design

4.1 Datasets

We conduct our experiments using PyTorch (Paszke et al., 2019) on two large-scale datasets that consist of physiological time-series, such as the electrocardiogram (ECG), alongside cardiac arrhythmia labels. **Chapman** (Zheng et al., 2020) consists of 12-lead ECG recordings from 10,646 patients alongside labels which we group into 4 major classes. **PTB-XL** (Wagner et al., 2020) consists of 12-lead ECG recordings from 18,885 patients alongside labels which we group into 5 major classes (Strodthoff et al., 2020). Further details can be found in Appendix B.

4.2 Deploying Clinical Prototypes for Retrieval

We aim to exploit clinical prototypes for retrieval and clustering purposes. To perform retrieval, we treat the CPs as the query set and retrieve the closest instances (↓ Euclidean distance) from a held-out dataset. In evaluating this task of retrieval, we deploy a commonly used metric known as Recall at K (R@K). This metric quantifies whether at least one of the K retrieved instances matches the query. In our context, however, a match can occur according to any of the three attributes: class, sex, and age. Therefore, we extract a single attribute, α_m, from the set of attributes, A, for each of the M clinical prototypes, and the same attribute, α_i, for each of the K retrieved instances, and define the following *attribute-specific* R@K.

$$\text{R@}K(\alpha) = \frac{1}{M} \sum_{m=1}^{M} \delta \left(\sum_{i=1}^{K} \delta(\alpha_i = \alpha_m) \geq 1 \right) \tag{8}$$

4.3 Deploying Clinical Prototypes for Clustering

Clinical prototypes, in addition to their role in retrieval, can be exploited for clustering. From this perspective, CPs can be thought of as multiple centroids belonging to a particular cluster. To evaluate these clusters, we first calculate the pairwise Euclidean distance between each representation and CP. We then assign each representation to the specific attribute, α_i^{pred}, of the CP to which it is closest. Given the ground-truth attribute for each representation, α_i^{true}, we can calculate the accuracy, $\text{Acc}(\alpha)$, of the assignments. We can also quantify the agreement between the attribute assignments of the ground-truth, $\vec{\alpha}^{true} = \{\alpha_{true}^1, \alpha_{true}^2, \ldots, \alpha_{true}^N\}$, and those obtained via clustering, $\vec{\alpha}^{pred} = \{\alpha_{pred}^1, \alpha_{pred}^2, \ldots, \alpha_{pred}^N\}$, by calculating the adjusted mutual information $\text{AMI}(\alpha) \in [0, 1]$.

$$\text{Acc}(\alpha) = \frac{1}{N} \sum_{i=1}^{N} \delta(\alpha_i^{pred} = \alpha_i^{true}) \tag{9}$$

$$\text{AMI}(\alpha) = \frac{\left[\text{MI}(\vec{\alpha}^{true}, \vec{\alpha}^{pred}) - \mathbb{E}(\text{MI}(\vec{\alpha}^{true}, \vec{\alpha}^{pred}))\right]}{\mathbb{E}(\text{H}(\vec{\alpha}^{true}), \text{H}(\vec{\alpha}^{pred})) - \mathbb{E}(\text{MI}(\vec{\alpha}^{true}, \vec{\alpha}^{pred}))} \tag{10}$$

where $\text{MI}(\vec{\alpha}^{true}, \vec{\alpha}^{pred})$ represents the mutual information between the ground-truth and the predicted set of attributes, and $\text{H}(\vec{\alpha})$ represents the entropy of the set of attributes.

4.4 Baselines

In the clustering scenario, we compare our method to the following approaches: 1) **K-Means** implements Expectation Maximization to arrive at class-specific centroids. Instances are then assigned to the class of their nearest centroid. We perform K-Means a) on the input instances (**K-Means Raw**) and b) on representations of instances learned using $\mathcal{L}_{contrastive-soft} + \mathcal{L}_{regression}$ (**K-Means Combined**). 2) **DeepCluster** (Caron et al., 2018) is an iterative method that performs K-Means on representations, pseudo-labels instances according to their assigned cluster, and then exploits such labels for supervised training. The final set of instance labels is taken from the epoch with the lowest validation loss. 3) **Information Invariant Clustering (IIC)** (Ji et al., 2019) maximizes the mutual information between the posterior class probabilities assigned to an instance and its perturbed counterpart. We adapt IIC to the time-series domain by perturbing instances with additive Gaussian noise, $\epsilon \sim \mathcal{N}(0, \sigma)$. We also incorporate auxiliary over-clustering as it was shown to significantly improve performance. The final set of instance labels is chosen by taking the argmax of the output probabilities. 4) **SeLA** (Asano et al., 2020) pseudo-labels instances by implementing the Sinkhorn-Knopp algorithm to allow for supervised training. We pseudo-label instances after each epoch of training and use prior class information to determine the number of clusters, which should boost performance.

4.5 Hyperparameters

We chose the temperature parameters, $\tau = 0.1$, as per (Kiyasseh et al., 2020), and $\tau_w = 1$. The regression regularization term (Eq. 6) requires the specification of β. We chose $\beta = 0.2$ due to our choice of distance metric (squared Euclidean distance) and the number of attribute groups. If β were too small in magnitude, the intra-cluster separability of clinical prototypes would be too small (see Appendix A). If β were too large, then the clinical prototypes from *different* classes would begin to overlap with one another and class separability diminishes. For both datasets, $\text{sex} \in \{\text{M}, \text{F}\}$, and age is converted to quartiles. For the Chapman and PTB-XL datasets, $M = |\text{class}| \times |\text{sex}| \times |\text{age}| = 32$ and 40, respectively. Further implementation details can be found in Appendix C.

5 Experimental Results

5.1 Deploying Clinical Prototypes for Retrieval

We exploit CPs to retrieve attribute-specific physiological signals from a database. In this section, we task the CPs with retrieving the closest $K = [1, 5, 10]$ instances in a held-out set and, in Table 1, illustrate the resulting $\text{R@}K$. We also stratify the results according to the number of matched

Table 1: Retrieval performance of DROPS implementation on Chapman and PTB-XL datasets for $K = 1, 5, 10$. Results are stratified according to the number of matched attributes between the query (CP) and retrieved instances and are averaged across 5 seeds.

	Chapman			PTB-XL		
# of matched attributes	$K = 1$	5	10	1	5	10
≥ 1	76.3	99.4	100	70	100	100
≥ 2	26.9	74.4	93.8	19.5	60	82
$= 3$	2.5	12.5	21.3	2.5	7	10

attributes between the query (CPs) and retrieved instances. For example, # of matched attributes $= 3$ implies that a perfect match has occurred for all attributes: class, sex, and age.

In Table 1, we show that clinical prototypes perform well in retrieving instances with at least one attribute match. This can be seen for # of matched attributes ≥ 1 where R@1$= 76.3$ and 70 for the Chapman and PTB-XL datasets, respectively. In the former case, this implies that 76.3% of the CPs retrieved an instance that had at least one match. We also find that as the number of retrieved instances increases ($\uparrow K$), so does the likelihood of obtaining one that has at least one attribute match. For example, as $K = 1 \rightarrow 10$, the R@$K = 76.3 \rightarrow 100$ on the Chapman dataset. Such a finding illustrates the potential utility of clinical prototypes as tools for retrieval.

On the other hand, we find that, when deployed to retrieve a single instance ($K = 1$), clinical prototypes struggle to retrieve one whose attribute sets match more than once. This is shown by R@1$= 26.9$ and 19.5 for the Chapman and PTB-XL datasets, respectively when the # of matched attributes ≥ 2. However, this struggle is significantly alleviated as more instances are retrieved. For example, for the Chapman dataset, as $K = 1 \rightarrow 10$, the R@$K = 26.9 \rightarrow 93.8$. In other words, when retrieving ten instances, 93.8% of the CPs find one whose attribute set matches at least twice. On a similar note, we find that in searching for a larger # of attributes that match, the retrieval performance of the clinical prototypes decreases (R@1$= 76.3 \rightarrow 2.5$). We hypothesize that this behaviour is due to our training paradigm's preference for the discrimination of classes over that of the remaining attributes. Therefore, perfect matches are more likely to occur for the class attribute. Nonetheless, the task of discriminating ECG recordings according to sex, for example, is notoriously difficult (Attia et al., 2019).

To qualitatively evaluate the retrieval capabilities of our clinical prototypes, we choose CPs at random to form the query set, calculate their Euclidean distance to the representations of instances in a *held-out* dataset, and retrieve the 5 which are closest. In Fig. 2, we visualize the ECG signals that correspond to these closest representations and colour their borders green if their class label matches that of the query, and red otherwise. We can see that at least 60% of the retrieved instances match the class label.

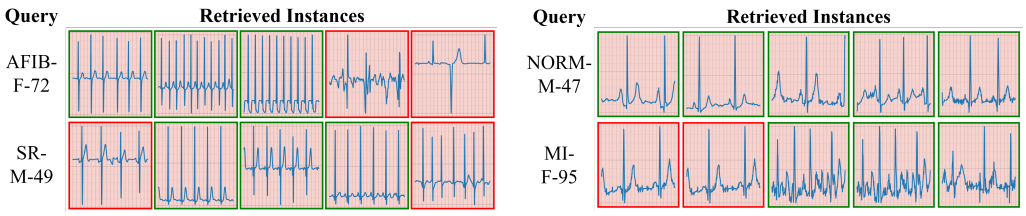

(a) Chapman (b) PTB-XL

Figure 2: Top 5 retrieved instances based on query CPs from the (a) Chapman and (b) PTB-XL datasets. Green and red borders indicate retrieved instances whose ground-truth class attribute matches that of the CPs and those whose ground-truth class attribute does not match, respectively.

5.2 DEPLOYING CLINICAL PROTOTYPES FOR CLUSTERING

So far, we have illustrated the utility of exploiting clinical prototypes for retrieval purposes. In this section, we evaluate the utility of CPs for clustering. In Table. 2, we illustrate the clustering performance of DROPS relative to that of state-of-the-art clustering methods.

Table 2: Accuracy and AMI between the labels assigned to representations in the validation set and the ground-truth (a) class attribute and (b) sex and age attributes. Results are shown across 5 seeds.

(a) Cardiac arrhythmia class attribute

Method	Chapman		PTB-XL	
	Acc	AMI	Acc	AMI
Unsupervised Clustering				
K-Means Raw	29.2	0.3	-	-
SeLA (Asano et al., 2020)	21.0	10.2	10.5	1.6
IIC (Ji et al., 2019)	27.0	0.2	22.0	0.5
DeepCluster (Caron et al., 2018)	32.3	3.0	10.5	4.9
Supervised Clustering				
K-Means Combined	81.7	61.9	36.5	27.4
DROPS Contrastive	89.8	72.1	76.1	36.0
DROPS Combined	**90.3**	**72.8**	**76.0**	**35.9**

(b) Sex and age attributes

Method	Chapman		PTB-XL	
	Sex	Age	Sex	Age
DROPS Contrastive	56.8	37.4	**74.3**	19.3
DROPS Combined	**57.4**	**38.0**	73.5	**19.5**

There are several takeaways from Table 2. First, our supervised contrastive learning paradigm generates rich representations. This can be seen by the superiority of K-Means Combined over K-Means Raw where the Acc(class) $= 81.7$ and 29.2, respectively. Note that this approach does *not* yet exploit clinical prototypes and thus allows for the reliable evaluation of the representations alone. We provide further evidence in support of the richness of these representations in Sec. 5.3. Second, we find that leveraging clinical prototypes, as is done with DROPS, builds upon the rich representations and further improves clustering performance. This can be seen by the performance of DROPS Combined which achieves an Acc(class) $= 90.3$ and 76.0 on the Chapman and PTB-XL datasets, respectively which outperforms not only its K-Means counterpart but also recent state-of-the-art methods such as DeepCluster, IIC, and SeLA. Such a finding underscores the vital role clinical prototypes play in clustering. We also note that our method can be trivially incorporated into DeepCluster, for example, to generate pseudo-labels. Lastly, in Table 2b, we show that DROPS is flexible enough to *simultaneously* cluster according to *multiple* attributes, a feature that does not trivially extend to other methods. Such flexibility can provide researchers with improved control over sensitive attributes.

5.3 CAPTURING SEMANTIC RELATIONSHIPS BETWEEN CLINICAL PROTOTYPES

Up until now, we have shown that clinical prototypes can be successfully deployed for retrieval and clustering. We encouraged such prototypes to exhibit inter and intra-cluster separability, with the aim of capturing semantic relationships between them. In this section, we look to confirm whether such semantic relationships are indeed captured. In Fig. 3 (Top Row), we illustrate the t-SNE projection of representations in the training set alongside the *average* class-specific CP. In Fig. 3 (Bottom Row), we illustrate the t-SNE projection of the CPs colour-coded and shaded according to sex and age groups, respectively. For clarity, we follow the same coding scheme presented in Fig. 1 (left).

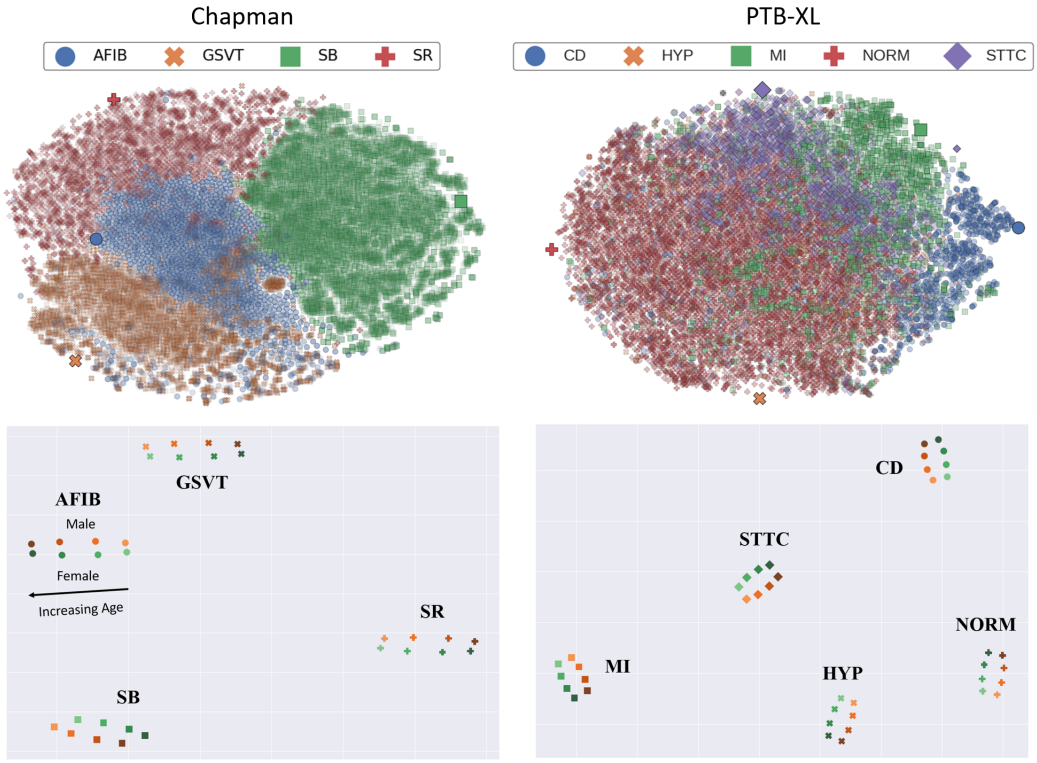

Figure 3: **Top Row**. t-SNE projection of the the representations in the training set of the Chapman and PTB-XL datasets, respectively, alongside the average clinical prototype *per class* (shown in larger size). **Bottom Row**. t-SNE projection of the corresponding clinical prototypes colour-coded and shaded according to sex and age, respectively (see Fig. 1 left).

We show that our training paradigm leads to clinical prototypes that can satisfy the semantic relationships between the class, sex, and age attributes. This can be seen by the high separability between, and ordering of, the sex and age attributes in Fig. 3 (Bottom Row). This observation holds regardless of the class attribute or the dataset that is experimented with. We further note the high degree of similarity between these projections, empirically-derived, and expected (see Fig. 1 left). We claim that the adoption of this formation by the CPs is driven primarily by our weighting mechanism (Eq. 3) and distance-based regularization term (Eq. 6). Empirical support for this claim can be found in Appendix A.

6 Discussion and Future Work

In this paper, we propose a supervised contrastive learning framework, DROPS, for the retrieval and clustering of physiological signals. In the process, we learn representations, entitled clinical prototypes, that efficiently describe the state of a patient associated with a set of attributes, e.g., disease, sex, and age. We show that clinical prototypes can capture semantic relationships and allow for the learning of rich representations advantageous for both the retrieval and clustering of physiological signals. We now elucidate several avenues worth exploring.

Learning Disentangled Clinical Prototypes. CPs are attribute-specific representations. Disentangling these representations into their constituent attributes might facilitate the interpretability of CPs and their application to fair ML. Preliminary exploratory work is performed in Appendix D.

Incorporate Continuous Attributes. CPs are currently limited to discrete attributes. Scaling CPs to a continuous set and large number of attributes will allow for more fine-grained retrieval and further increase their utility.

REFERENCES

Yuki Asano, Christian Rupprecht, and Andrea Vedaldi. Self-labelling via simultaneous clustering and representation learning. In *International Conference on Learning Representations*, 2020. URL https://openreview.net/forum?id=Hyx-jyBFPr.

Zachi I Attia, Paul A Friedman, Peter A Noseworthy, Francisco Lopez-Jimenez, Dorothy J Ladewig, Gaurav Satam, Patricia A Pellikka, Thomas M Munger, Samuel J Asirvatham, Christopher G Scott, et al. Age and sex estimation using artificial intelligence from standard 12-lead ecgs. *Circulation: Arrhythmia and Electrophysiology*, 12(9):e007284, 2019.

Siddharth Biswal, Cao Xiao, Lucas M Glass, Elizabeth Milkovits, and Jimeng Sun. Doctor2vec: Dynamic doctor representation learning for clinical trial recruitment. In *Proceedings of the AAAI Conference on Artificial Intelligence*, volume 34, pp. 557–564, 2020.

Mathilde Caron, Piotr Bojanowski, Armand Joulin, and Matthijs Douze. Deep clustering for unsupervised learning of visual features. In *Proceedings of the European Conference on Computer Vision (ECCV)*, pp. 132–149, 2018.

Steve R Chamberlin, Steven D Bedrick, Aaron M Cohen, Yanshan Wang, Andrew Wen, Sijia Liu, Hongfang Liu, and William Hersh. Evaluation of patient-level retrieval from electronic health record data for a cohort discovery task. *medRxiv*, pp. 19005280, 2019.

Deepak Roy Chittajallu, Bo Dong, Paul Tunison, Roddy Collins, Katerina Wells, James Fleshman, Ganesh Sankaranarayanan, Steven Schwaitzberg, Lora Cavuoto, and Andinet Enquobahrie. Xai-cbir: Explainable ai system for content based retrieval of video frames from minimally invasive surgery videos. In *2019 IEEE 16th International Symposium on Biomedical Imaging (ISBI 2019)*, pp. 66–69. IEEE, 2019.

Sajad Darabi, Mohammad Kachuee, Shayan Fazeli, and Majid Sarrafzadeh. Taper: Time-aware patient ehr representation. *IEEE Journal of Biomedical and Health Informatics*, 2020.

Leonard W D'Avolio, Thien M Nguyen, Wildon R Farwell, Yongming Chen, Felicia Fitzmeyer, Owen M Harris, and Louis D Fiore. Evaluation of a generalizable approach to clinical information retrieval using the automated retrieval console (arc). *Journal of the American Medical Informatics Association*, 17(4):375–382, 2010.

European Commission. exchange-electronic-health-records-across-eu, 2019. URL https://ec.europa.eu/digital-single-market/en/exchange-electronic-health-records-across-eu.

Vivien Sainte Fare Garnot and Loic Landrieu. Metric-guided prototype learning, 2020.

Travis R Goodwin and Sanda M Harabagiu. Learning relevance models for patient cohort retrieval. *JAMIA open*, 1(2):265–275, 2018.

Harsha Gurulingappa, Luca Toldo, Claudia Schepers, Alexander Bauer, and Gerard Megaro. Semi-supervised information retrieval system for clinical decision support. In *TREC*, 2016.

William R Hersh and Robert A Greenes. Information retrieval in medicine: state of the art. *MD Computing: Computers in Medical Practice*, 7(5):302–311, 1990.

Li Huang, Andrew L Shea, Huining Qian, Aditya Masurkar, Hao Deng, and Dianbo Liu. Patient clustering improves efficiency of federated machine learning to predict mortality and hospital stay time using distributed electronic medical records. *Journal of biomedical informatics*, 99:103291, 2019.

Xu Ji, João F Henriques, and Andrea Vedaldi. Invariant information clustering for unsupervised image classification and segmentation. In *Proceedings of the IEEE International Conference on Computer Vision*, pp. 9865–9874, 2019.

Alistair EW Johnson, Tom J Pollard, Lu Shen, H Lehman Li-Wei, Mengling Feng, Mohammad Ghassemi, Benjamin Moody, Peter Szolovits, Leo Anthony Celi, and Roger G Mark. Mimic-iii, a freely accessible critical care database. *Scientific Data*, 3(1):1–9, 2016.

Dani Kiyasseh, Tingting Zhu, and David A Clifton. Clocs: Contrastive learning of cardiac signals. *arXiv preprint arXiv:2005.13249*, 2020.

Matt J Kusner, Joshua Loftus, Chris Russell, and Ricardo Silva. Counterfactual fairness. In *Advances in neural information processing systems*, pp. 4066–4076, 2017.

Isotta Landi, Benjamin S Glicksberg, Hao-Chih Lee, Sarah Cherng, Giulia Landi, Matteo Danieletto, Joel T Dudley, Cesare Furlanello, and Riccardo Miotto. Deep representation learning of electronic health records to unlock patient stratification at scale. *arXiv preprint arXiv:2003.06516*, 2020.

Junnan Li, Pan Zhou, Caiming Xiong, Richard Socher, and Steven CH Hoi. Prototypical contrastive learning of unsupervised representations. *arXiv preprint arXiv:2005.04966*, 2020a.

Yue Li, Pratheeksha Nair, Xing Han Lu, Zhi Wen, Yuening Wang, Amir Ardalan Kalantari Dehaghi, Yan Miao, Weiqi Liu, Tamas Ordog, Joanna M Biernacka, et al. Inferring multimodal latent topics from electronic health records. *Nature Communications*, 11(1):1–17, 2020b.

Dianbo Liu, Dmitriy Dligach, and Timothy Miller. Two-stage federated phenotyping and patient representation learning. *arXiv preprint arXiv:1908.05596*, 2019.

Riccardo Miotto, Li Li, Brian A Kidd, and Joel T Dudley. Deep patient: an unsupervised representation to predict the future of patients from the electronic health records. *Scientific Reports*, 6(1): 1–10, 2016.

Adam Paszke, Sam Gross, Francisco Massa, Adam Lerer, James Bradbury, Gregory Chanan, Trevor Killeen, Zeming Lin, Natalia Gimelshein, Luca Antiga, et al. Pytorch: An imperative style, high-performance deep learning library. In *Advances in Neural Information Processing Systems*, pp. 8024–8035, 2019.

Adam M. Rhine. *Information Retrieval for Clinical Decision Support*. PhD thesis, 2017.

R Rani Saritha, Varghese Paul, and P Ganesh Kumar. Content based image retrieval using deep learning process. *Cluster Computing*, 22(2):4187–4200, 2019.

Yuqi Si and Kirk Roberts. Deep patient representation of clinical notes via multi-task learning for mortality prediction. *AMIA Summits on Translational Science Proceedings*, 2019:779, 2019.

Nils Strodthoff, Patrick Wagner, Tobias Schaeffter, and Wojciech Samek. Deep learning for ECG analysis: Benchmarks and insights from PTB-XL. *arXiv preprint arXiv:2004.13701*, 2020.

Arnaud Van Looveren and Janis Klaise. Interpretable counterfactual explanations guided by prototypes. *arXiv preprint arXiv:1907.02584*, 2019.

Sahil Verma and Julia Rubin. Fairness definitions explained. In *2018 IEEE/ACM International Workshop on Software Fairness (FairWare)*, pp. 1–7. IEEE, 2018.

Patrick Wagner, Nils Strodthoff, Ralf-Dieter Bousseljot, Wojciech Samek, and Tobias Schaeffter. PTB-XL, a large publicly available electrocardiography dataset, 2020. URL `https://physionet.org/content/ptb-xl/1.0.1/`.

Byron C Wallace, Joël Kuiper, Aakash Sharma, Mingxi Zhu, and Iain J Marshall. Extracting pico sentences from clinical trial reports using supervised distant supervision. *The Journal of Machine Learning Research*, 17(1):4572–4596, 2016.

Haolin Wang, Qingpeng Zhang, and Jiahu Yuan. Semantically enhanced medical information retrieval system: a tensor factorization based approach. *IEEE Access*, 5:7584–7593, 2017.

Yanshan Wang, Andrew Wen, Sijia Liu, William Hersh, Steven Bedrick, and Hongfang Liu. Test collections for electronic health record-based clinical information retrieval. *JAMIA open*, 2(3): 360–368, 2019.

Jianwei Zheng, Jianming Zhang, Sidy Danioko, Hai Yao, Hangyuan Guo, and Cyril Rakovski. A 12-lead electrocardiogram database for arrhythmia research covering more than 10,000 patients. *Scientific Data*, 7(1):1–8, 2020.